JOURNAL OF SPACECRAFT AND ROCKETS
Vol. 35, No. 2, March–April 1998

Buckling and Quasistatic Thermal–Structural Response of Asymmetric Rolled-Up Solar Array

Masahiko Murozono*
Kyushu University, Fukuoka 812, Japan
and
Earl A. Thornton†
University of Virginia, Charlottesville, Virginia 22903

Analytical studies for buckling and the quasistatic thermal–structural response of an asymmetrical rolled-up solar array of the type used on the Hubble Space Telescope are presented. A buckling analysis assuming asymmetric loading because of geometric asymmetry establishes critical buckling forces and buckling modes. Quasistatic thermal–structural responses of the solar array subjected to the sudden radiation heating typical of a night–day orbital transition are also developed. Computations conducted for the Hubble Space Telescope show that the solar arrays were deployed with a solar blanket prestress that would induce global torsional buckling. Numerical computations for the quasistatic response show that thermally induced bending–torsional deformations would cause bending moments in the solar array's booms consistent with the local buckling failure observed by the astronauts.

Nomenclature

A	= two-element storable tubular extendable member (BiSTEM) cross-sectional area, m^2
b	= half spreader bar width, m
$b_1 + b_2$	= solar blanket width, m
C_{ij} $(i, j = 1, 2)$	= coefficients of buckling equation; see Eqs. (24) and (28)
c	= BiSTEM specific heat, J/(kg · K)
d	= solar blanket fixed end offset, m
EI	= BiSTEM bending stiffness, N · m^2
$E\Gamma$	= BiSTEM warping stiffness, N · m^4
F_x	= solar blanket tension, N/m
GJ	= BiSTEM torsional stiffness, N · m^2
g_1, g_2	= nonhomogeneous term due to thermal effects; see Eq. (46)
h	= BiSTEM wall thickness, m
I_E	= BiSTEM polar moment of inertia, m^4
k	= BiSTEM thermal conductivity, W/(m · K)
L	= solar array length, m
M_T	= thermal bending moment, N · m
M_{x1}, M_{x2}	= BiSTEM torque, N · m
M_1, M_2	= BiSTEM bending moment, N · m
P	= BiSTEM average axial force, N
P_{cr}	= critical buckling force, N
P_{f1}, P_{f2}	= ratios of P_1 and P_2 to P
P_1, P_2	= BiSTEM axial force, N
R	= BiSTEM radius, m
s_0	= solar heat flux, W/m^2
T	= temperature, K
$\bar{T}$	= average temperature, K
T_m	= perturbation temperature, K
$\bar{T}_{ss}$	= steady-state average temperature, K
T^*	= steady-state perturbation temperature, K
t	= time, s
V_1, V_2	= BiSTEM shear force, N
w_m	= solar blanket deflection, m
w_s	= spreader bar deflection, m
w_{s0}, θ_{s0}	= center of spreader bar deflection and rotation
w_1, w_2	= BiSTEM deflection, m
x, y, z	= solar array coordinates, m
x_m	= maximum bending moment position, m
α	= BiSTEM coefficient of thermal expansion, 1/K
α_s	= BiSTEM thermal absorptivity
α_1, α_2	= magnitude of BiSTEM deflection, m
β_i, β_i' $(i = 1, 2)$	= torsional buckling eigenvalue [see Eq. (12)], 1/m
γ_1, γ_2	= magnitude of BiSTEM angle of twist, rad
δ	= Kronecker delta function
ε_s	= BiSTEM thermal emissivity
θ_{x1}, θ_{x2}	= BiSTEM angle of twist, rad
λ_1, λ_2	= bending buckling eigenvalue [see Eq. (8)], 1/m
ρ	= BiSTEM density, kg/m^3
σ	= Stefan–Boltzmann constant, W/(m^2 · K^4)
υ	= thermal response time, s
χ	= BiSTEM angular coordinate, rad

Received March 11, 1997; revision received Sept. 22, 1997; accepted for publication Sept. 23, 1997.

*Associate Professor, Department of Aeronautics and Astronautics, 6-10-1 Hakozaki, Higashi-ku. Member AIAA.

†Professor and Director, Light Thermal Structures Center. Associate Fellow AIAA.

Introduction

THE Hubble Space Telescope (HST) was launched into low Earth orbit aboard the Space Shuttle Discovery on flight STS-31 in April 1990, and the next day the HST was deployed successfully from the Discovery payload bay. The problem of the spherical aberration of the spacecraft mirror was discovered within a short time after initial imaging data were acquired. Another spacecraft problem, a pointing jitter induced by thermal bending of the solar arrays, was also discovered during the initial checkout period. The vibrations were induced when the solar array structure was exposed to a sudden temperature change as the spacecraft passed through a night–day orbital transition. The solar arrays were developed by the European Space Agency and were based on a flexible rolled-up solar array (FRUSA) concept. Each solar array consists of a flexible solar blanket and two two-element storable tubular extendable members (BiSTEMs), both of which were originally furled within a drum at launch. Early analyses of the jitter problem indicated that the solar array oscillations were related to thermally induced bending of the BiSTEMs. In December 1993, the HST was repaired in orbit 590 km above Earth by astronauts aboard the Space Shuttle Endeavour. The replacement of the solar arrays was among the most important task of the mission. When the astronauts began to replace the solar arrays, it became clear that a BiSTEM of one solar array was damaged with a kink about midway along its length. Though other solar arrays were retracted into their storage canisters prior to their replacement according to the mission plan, the damaged solar array

could not be retracted, and it was jettisoned. Photographs of the solar arrays taken by the astronauts indicated an unexpected twisting of the solar arrays, for example, see Refs. 1 and 2.

There were clearly some problems with the thermal–structural design of the HST solar arrays that led to the vibration problem and the BiSTEM failure. However, not many details are available in the public domain. Several engineering questions still remain. Is the failure of the solar array BiSTEM related to the twisting behavior, and what is the role of the thermal effect? Chaisson[3] describes the sequence of events that led to the identification of solar array as the cause of the HST pointing jitter problem. Thornton and Kim[4] describe an analysis of the thermal–structural responses of a symmetric FRUSA model for a typical night–day transition. Uncoupled and coupled thermal–structural dynamic responses were studied using an analytical model restricted to symmetric bending deformations of the solar array. They calculated buckling forces, natural frequencies, and modes for bending vibration and obtained the temperature histories as well as quasistatic and dynamic structural responses based on the uncoupled analysis. The stability criterion for thermal flutter was also established by a coupled thermal–structural analysis. However, the critical bending buckling force was more than three times the HST BiSTEM's compressive force. Chung and Thornton[5] focused on a torsional analysis of a symmetric FRUSA model. A torsional buckling analysis was conducted using an analytical model restricted to antisymmetric torsional deformations of the solar array. Effects of initial imperfections on the torsional deformation and natural vibrations in the torsional mode were also presented. The torsional buckling force was approximately equal to the HST BiSTEM's compressive force, which suggests a relation between the BiSTEM failure and torsional buckling. However, examination of the HST solar array geometry suggests that it is important to consider the asymmetry of the solar array. An HST solar array is not exactly symmetric about its centerline; its solar blanket is shifted slightly toward the outer BiSTEM. Even though the solar array was heated by uniform radiation, coupled bending–torsional deformations occur because of the asymmetry.

This paper describes buckling analyses and quasistatic thermal–structural analyses of an asymmetric FRUSA model to determine a better understanding of the causes of the HST's vibration and failure problems. Buckling analyses considering the geometric asymmetry establish solar array critical buckling forces and buckling modes. The effect of the offset of the fixed supported end of the solar blanket on the bending–torsional coupling deformations of the solar array is investigated. Moreover, quasistatic structural responses of the solar array subject to sudden radiant heating for a typical night–day orbital transition are also presented. Variations of the deflection and the bending moment of the BiSTEM with axial compressive force are calculated, and the cause of the failure of the solar array BiSTEM of the HST is discussed.

Solar Array Model

The HST solar array in-orbit configuration consists of two identical winglike structures. Each wing has two flexible solar blankets that are deployed from a drum mounted on a shaft cantilevered from the spacecraft. Each solar blanket is unfurled by a rotating actuator mechanism that pushes the two BiSTEM booms from the drum. The deployed ends of the BiSTEMs are connected to a spreader bar to which one end of the solar blanket is attached. A BiSTEM is made from thin stainless-steel tapes formed into circular open cross sections. In their stored configuration, each tape is flattened and stored on a spool within the drum mechanism. During deployment, the stored elastic energy in the flattened tape assists the unfurling mechanisms as each STEM extends and curls back to its original shape, with seams diametrically opposed, forming a BiSTEM. The spreader bar houses a mechanism that compensates for a difference in the BiSTEMs lengths. The storage drum houses a torque mechanism that maintains blanket tension. Thus, during orbital operations, the blanket tension on the spreader bar exerts a compressive force on each BiSTEM.

The mathematical model and coordinate system used in the subsequent analyses are shown in Fig. 1. The model assumes that 1) the solar blanket is an inextensible membrane whose thermal expansions and contractions are neglected, 2) the solar blanket is subjected to uniform tension in the x direction and the membrane tensile force F_x per unit width is constant, 3) the inner and outer BiSTEM booms are identical cantilevered beams subjected to different axial compressive forces P_1 and P_2, respectively, 4) torsional rotations are sufficiently small so that the BiSTEMs' bending displacements occur only in the $x-z$ plane, 5) thermal expansions of the BiSTEMs are neglected, and 6) the spreader bar is a rigid member of length $2b$ and supports the membrane tensile force over a length $b_1 + b_2$. For the determination of the temperature distributions, the BiSTEM booms are assumed to be one-piece, thin-walled circular section beams.

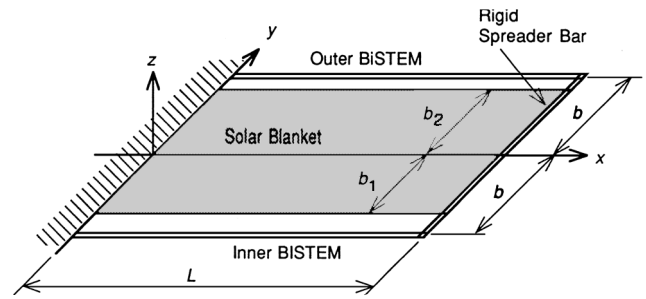

Fig. 1 Solar array analytical model.

Buckling Analysis

For the buckling analysis, two models are employed. In the first model, the fixed end of the solar blanket at $x = 0$ is assumed to lie in the $x-y$ plane, as shown in Fig. 1. This model is an idealization of the HST solar array, where there is an offset of the solar blanket so that the support at $x = 0$ is offset a small distance d above the y axis. In the second model, the blanket offset is considered.

Without Blanket Offset

When the solar blanket is subjected to uniform tensile forces F_x per unit length, the axial compressible forces on the two BiSTEMs are assumed to be represented by P_1 and P_2, where subscripts 1 and 2 are the inner BiSTEM and the outer BiSTEM, respectively. Equilibrium of forces on the spreader bar in the x direction and equilibrium of moments about the z axis are presented by the following equations:

$$P_1 + P_2 - \int_{-b_1}^{b_2} F_x \, dy = 0 \tag{1}$$

$$P_1 b - P_2 b + \int_{-b_1}^{b_2} F_x y \, dy = 0 \tag{2}$$

Solving these equations for P_1 and P_2 yields

$$P_i = P_{fi} P, \qquad i = 1, 2 \tag{3a}$$

$$P_{f1} = 1 - \frac{b_2 - b_1}{2b} \tag{3b}$$

$$P_{f2} = 1 + \frac{b_2 - b_1}{2b} \tag{3c}$$

Nondimensional factors P_{fi} $(i = 1, 2)$ have values between 0.5 and 1.5 if we assume that $0 < b_1, b_2 < b$. An average axial compressive force P for the BiSTEMs is defined by

$$P = \tfrac{1}{2} F_x (b_1 + b_2) \tag{3d}$$

Considering effects of the compressive axial forces, the equation and the boundary conditions for a BiSTEM are described as bending of a Bernoulli–Euler beam:

$$EI \frac{d^4 w_i}{dx^4} + P_i \frac{d^2 w_i}{dx^2} = 0, \qquad i = 1, 2 \tag{4}$$

$$w_i(0) = 0, \qquad \frac{dw_i}{dx}(0) = 0, \qquad M_i(L) = 0 \tag{5}$$

where M_i is the BiSTEM boom bending moment defined by

$$M_i = -EI\frac{\mathrm{d}^2 w_i}{\mathrm{d}x^2} \tag{6}$$

Deflections of the BiSTEMs are obtained by solving Eq. (4) subject to the boundary conditions Eq. (5). The result is

$$w_i(x) = \alpha_i\{\tan\lambda_i L(1-\cos\lambda_i x) - (\lambda_i x - \sin\lambda_i x)\} \tag{7}$$

where α_i ($i = 1, 2$) in Eq. (7) are constants. Parameters λ_i ($i = 1, 2$) are defined by

$$\lambda_i^2 = P_i/EI = P_{fi}(P/EI) \tag{8}$$

The equation and the corresponding boundary conditions for BiSTEM torsion including the effects of axial compressive forces are expressed as

$$E\Gamma\frac{\mathrm{d}^4\theta_{xi}}{\mathrm{d}x^4} - \left(GJ - \frac{P_i I_E}{A}\right)\frac{\mathrm{d}^2\theta_{xi}}{\mathrm{d}x^2} = 0, \qquad i = 1, 2 \tag{9}$$

$$\theta_{xi}(0) = 0, \qquad \frac{\mathrm{d}\theta_{xi}}{\mathrm{d}x}(0) = 0, \qquad \frac{\mathrm{d}\theta_{xi}}{\mathrm{d}x}(L) = 0 \tag{10}$$

The latter two boundary conditions mean that the BiSTEM cross section is restrained from warping at both ends. There are two possible solutions to Eq. (9) under the boundary conditions equation (10) depending on the sign of β_i^2:

$$\theta_{xi}(x) = \gamma_i\{\sinh\beta_i L(\sinh\beta_i x - \beta_i x) - (1-\cosh\beta_i L)(1-\cosh\beta_i x)\} \tag{11a}$$

when $\beta_i^2 \geq 0$ and

$$\theta_{xi}(x) = \gamma_i\{\sin\beta_i' L(\sin\beta_i' x - \beta_i' x) + (1-\cos\beta_i' L)(1-\cos\beta_i' x)\} \tag{11b}$$

when $\beta_i^2 < 0$, where β_i and β_i' are defined by Eq. (12). If P_i is relatively small, it can be assumed that $\beta_i^2 > 0$, and then

$$\beta_i^2 = (1/E\Gamma)[GJ - (P_i I_E/A)] = (1/E\Gamma)[GJ - P_{fi}(PI_E/A)] \tag{12a}$$

$$\beta_i'^2 = -\beta_i^2 \tag{12b}$$

The constants γ_i ($i = 1, 2$) in the solutions for the BiSTEM angle of twist can be expressed in terms of α_i considering the geometrical restraint conditions for the rotations of the BiSTEM tips. That is, because we assume that the spreader bar is a rigid body, the angle of twist at the BiSTEM tips must be equal to the rigid rotation angle of the spreader bar (Fig. 2a). Then

$$\theta_{x1}(L) = \theta_{x2}(L) = (1/2b)\{w_2(L) - w_1(L)\} \tag{13}$$

Substituting Eqs. (7) and (11), the constants γ_i are expressed, depending the sign of β_i^2, as

$$\gamma_i = \frac{1}{2b}\frac{\alpha_1(\tan\lambda_1 L - \lambda_1 L) - \alpha_2(\tan\lambda_2 L - \lambda_2 L)}{\beta_i L\sinh\beta_i L + 2(1-\cosh\beta_i L)} \tag{14a}$$

when $\beta_i^2 \geq 0$ and

$$\gamma_i = \frac{1}{2b}\frac{\alpha_1(\tan\lambda_1 L - \lambda_1 L) - \alpha_2(\tan\lambda_2 L - \lambda_2 L)}{\beta_i' L\sin\beta_i' L - 2(1-\cos\beta_i' L)} \tag{14b}$$

when $\beta_i'^2 = -\beta_i^2 > 0$.

The solar blanket is modeled as a membrane with constant tension F_x. Because the membrane has a high aspect ratio and the transverse edges of the membrane are free, the tension F_y that is perpendicular to F_x is neglected. Because the solar blanket is free from transverse pressure, the classical equilibrium equation for a membrane reduces to

$$F_x\frac{\partial^2 w_m}{\partial x^2} = 0 \tag{15}$$

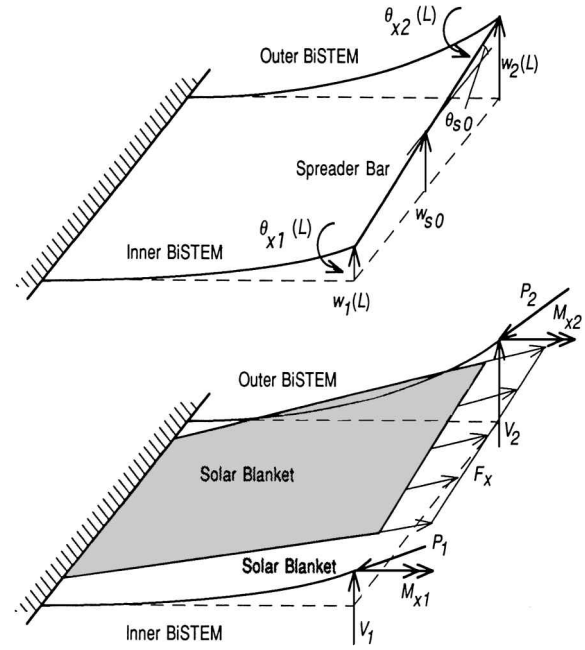

a) BiSTEMs and solar blanket

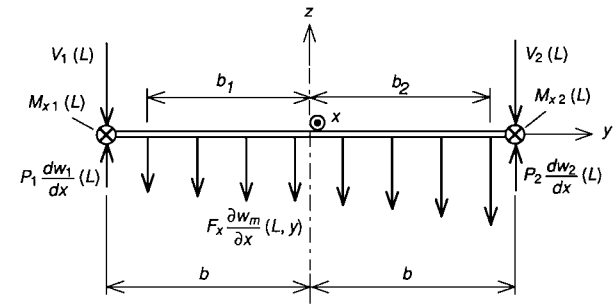

b) Forces on spreader bar

Fig. 2 Displacements and forces of the solar array elements.

and the boundary conditions are

$$w_m(0, y) = 0, \qquad w_m(L, y) = w_s(y) \tag{16}$$

Because we assume the spreader bar is rigid, w_s may be written using the deflection of its center of mass w_{s0} and the rigid rotation angle of the spreader bar θ_{s0}:

$$w_s(y) = w_{s0} + y\theta_{s0} \tag{17}$$

For small rotations, the deflection and the rotation of the spreader bar are expressed using the tip deflections of the BiSTEMs:

$$w_{s0} = \tfrac{1}{2}\{w_1(L) + w_2(L)\} \tag{18a}$$

$$\theta_{s0} = (1/2b)\{w_2(L) - w_1(L)\} \tag{18b}$$

Solving Eq. (15) subject to the boundary conditions equation (16) and using the preceding three equations, the solar blanket deflection can be written as

$$w_m(x, y) = \tfrac{1}{2}(x/L) \times [\{\alpha_2(\tan\lambda_2 L - \lambda_2 L) - \alpha_1(\tan\lambda_1 L - \lambda_1 L)\}(y/b) + \{\alpha_1(\tan\lambda_1 L - \lambda_1 L) + \alpha_2(\tan\lambda_2 L - \lambda_2 L)\}] \tag{19}$$

Next, let us consider force and moment equilibrium of the spreader bar in each direction. First, from the force equilibrium in the x direction and moment equilibrium about the z axis, the relation between F_x and P is

$$F_x = \frac{2P}{b_1 + b_2} \tag{20}$$

Force equilibrium of the spreader bar in the z direction is obtained with reference to the free body diagram shown in Fig. 2b:

$$V_1(L) + V_2(L) + \int_{-b_1}^{b_2} F_x \frac{\partial w_m}{\partial x}(L, y)\,\mathrm{d}y - P_1 \frac{\mathrm{d}w_1}{\mathrm{d}x}(L) - P_2 \frac{\mathrm{d}w_2}{\mathrm{d}x}(L) = 0 \tag{21}$$

where V_i is defined by

$$V_i = -EI \frac{\mathrm{d}^3 w_i}{\mathrm{d}x^3} \tag{22}$$

Equation (7) for the BiSTEM deflection and Eq. (19) for the solar blanket deflection are used to express each term in Eq. (21) in terms of the α_i. Thus, we obtain the following equation for α_i:

$$C_{11}(P)\alpha_1 + C_{12}(P)\alpha_2 = 0 \tag{23}$$

where each coefficient C_{1i} $(i = 1, 2)$ is a function of P defined by

$$C_{11}(P) = P_{f1}P\lambda_1 + P\frac{\tan\lambda_1 L - \lambda_1 L}{L}\left(1 - \frac{b_2 - b_1}{2b}\right) \tag{24a}$$

$$C_{12}(P) = P_{f2}P\lambda_2 + P\frac{\tan\lambda_2 L - \lambda_2 L}{L}\left(1 + \frac{b_2 - b_1}{2b}\right) \tag{24b}$$

Finally, we consider moment equilibrium of the spreader bar about the x axis. We refer again to the free body diagram shown in Fig. 2b and obtain

$$M_{x1}(L) + M_{x2}(L) - bV_1(L) + bV_2(L) + bP_1\frac{\mathrm{d}w_1}{\mathrm{d}x}(L) - bP_2\frac{\mathrm{d}w_2}{\mathrm{d}x}(L) + \int_{-b_1}^{b_2} F_x \frac{\partial w_m}{\partial x}(L, y)\,y\,\mathrm{d}y = 0 \tag{25}$$

where the BiSTEM torque M_{xi} is defined by

$$M_{xi} = \left(GJ - \frac{P_i I_E}{A}\right)\frac{\mathrm{d}\theta_{xi}}{\mathrm{d}x} - E\Gamma\frac{\mathrm{d}^3\theta_{xi}}{\mathrm{d}x^3} \tag{26}$$

Each term in the preceding equation is expressed in terms of α_i, after substituting Eqs. (7) and (11) for the BiSTEM deflection and rotation, respectively, and Eq. (19) for the solar blanket deflection. We rearrange the expression and obtain, finally,

$$C_{21}(P)\alpha_1 + C_{22}(P)\alpha_2 = 0 \tag{27}$$

where coefficients C_{21} and C_{22} are functions of P, and if $\beta_i^2 > 0$ they are expressed as follows:

$$C_{21}(P) = P_{f1}Pb\lambda_1 + Pb\frac{\tan\lambda_1 L - \lambda_1 L}{L} \times \left(\frac{b_2^2 - b_1 b_2 + b_1^2}{3b^2} - \frac{b_2 - b_1}{2b}\right) + \frac{\tan\lambda_1 L - \lambda_1 L}{2b} \times \sum_{i=1}^{2}\left(GJ - P_{fi}\frac{PI_E}{A}\right)\frac{\beta_i \sinh\beta_i L}{\beta_i L \sinh\beta_i L + 2(1 - \cosh\beta_i L)} \tag{28a}$$

$$C_{22}(P) = -P_{f2}Pb\lambda_2 - Pb\frac{\tan\lambda_2 L - \lambda_2 L}{L} \times \left(\frac{b_2^2 - b_1 b_2 + b_1^2}{3b^2} + \frac{b_2 - b_1}{2b}\right) - \frac{\tan\lambda_2 L - \lambda_2 L}{2b} \times \sum_{i=1}^{2}\left(GJ - P_{fi}\frac{PI_E}{A}\right)\frac{\beta_i \sinh\beta_i L}{\beta_i L \sinh\beta_i L + 2(1 - \cosh\beta_i L)} \tag{28b}$$

If $\beta_i^2 < 0$, the terms including the hyperbolic functions in Eq. (28) are replaced by the term

$$\frac{\beta_i' \sin\beta_i' L}{\beta_i' L \sin\beta_i' L - 2(1 - \cos\beta_i' L)} \tag{28c}$$

including trigonometric functions.

With matrix notation, Eqs. (24) and (27) are expressed in concise form as

$$\begin{bmatrix} C_{11}(P) & C_{12}(P) \\ C_{21}(P) & C_{22}(P) \end{bmatrix}\begin{Bmatrix} \alpha_1 \\ \alpha_2 \end{Bmatrix} = \begin{Bmatrix} 0 \\ 0 \end{Bmatrix} \tag{29}$$

Both λ_i and β_i are defined in terms of the compressive axial force of the BiSTEM in Eqs. (8) and (12), respectively. Thus, the coefficients of the simultaneous equations C_{ij} are determined by the BiSTEM compressive axial forces, geometric and physical properties of the solar array. The characteristic equation for the critical buckling force is obtained as the expression that means a nontrivial solution for α_i exists in Eq. (29). That is, the determinant of the coefficient matrix of Eq. (29) must vanish:

$$\det[C_{ij}] = C_{11}C_{22} - C_{12}C_{21} = 0 \tag{30}$$

This relation is a transcendental equation for P, and we may solve it numerically for the critical buckling forces.

When the solar array is symmetric about its centerline, that is, when $b_1 = b_2 = b'$, the coefficients satisfy

$$C_{12} = C_{11}, \qquad C_{22} = -C_{21} \tag{31}$$

Therefore, the determinant in Eq. (30) becomes $\det[C_{ij}] = -2C_{11}C_{21}$, and the characteristic equation for the bending mode buckling forces and the characteristic equation for the torsional mode buckling forces are uncoupled. For bending, the critical buckling forces obtained from the equation $C_{11} = 0$ are

$$P_{\mathrm{cr}} = n^2(\pi^2 EI/L^2), \qquad n = 1, 2, 3, \ldots \tag{32}$$

These agree with the bending buckling forces of the symmetric solar array calculated in Ref. 4. If $\beta_i^2 > 0$, rearrangement of the equation $C_{21} = 0$ gives the following expression for the torsional buckling loads:

$$Pb\lambda + \frac{Pb'^2}{3bL}(\tan\lambda L - \lambda L) + \frac{(\beta/b)[GJ - (PI_E/A)](\tan\lambda L - \lambda L)}{\beta L + [(1 - \cosh\beta L)^2/\sinh\beta L] - \sinh\beta L} = 0 \tag{33}$$

This equation is the same as the characteristic equation for torsional buckling forces formulated in Ref. 5 for a symmetric solar array.

With Blanket Offset

With reference to Fig. 3, let us consider the case in which the solar blanket does not exist in the plane including the two BiSTEMs and the spreader bar. We assume that the fixed supported end of the solar blanket is located at a distance d out of the plane from the fixed ends of the BiSTEMs. Thus, the first equation of the boundary conditions of the solar blanket deflection, Eq. (16), is replaced with the following equation:

$$w_m(0, y) = d \tag{34}$$

A similar formulation was conducted considering this condition, assuming that the offset d is small so that $d/L \ll 1$ is satisfied. Finally, instead of Eq. (29) we obtain the following simultaneous equations:

$$\begin{bmatrix} C_{11}(P) & C_{12}(P) \\ C_{21}(P) & C_{22}(P) \end{bmatrix}\begin{Bmatrix} \alpha_1 \\ \alpha_2 \end{Bmatrix} = P\frac{d}{L}\begin{Bmatrix} 2 \\ b_1 - b_2 \end{Bmatrix} \tag{35}$$

where C_{ij} $(i, j = 1, 2)$ are the coefficients defined by Eqs. (24) and (28) and are functions of the average compressive axial force of the BiSTEM. By considering the deflection as the sum of a static

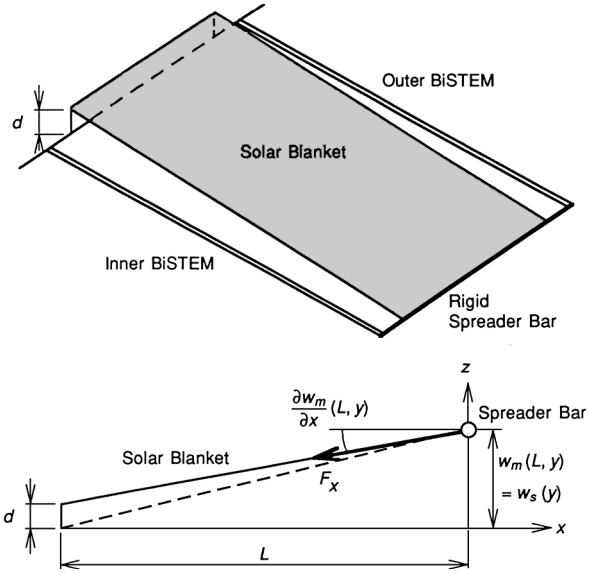

Fig. 3 Out-of-plane offset of solar blanket fixed supported end.

deflection and an increment due to the buckling deformation, it is shown that the critical buckling forces are calculated by the same characteristic equation $\det[C_{ij}] = 0$ as the case $d = 0$. That is, the small offset d does not affect the buckling forces. If $\det[C_{ij}] \neq 0$, Eq. (35) can be solved for α_i uniquely, and finite deflections are determined according to the value of the compressive force P. The existence of the offset d has similar effects as the existence of initial imperfections. Using α_i obtained by solving Eq. (35), deflections of the BiSTEMs are calculated by Eq. (7), and the rotations are calculated by Eq. (11) coupled with Eq. (14). Instead of Eq. (19), the solar blanket deflection is obtained by the following equation including the effects of the offset d:

$$w_m(x, y) = \tfrac{1}{2}(x/L)[\{\alpha_2(\tan\lambda_2 L - \lambda_2 L) - \alpha_1(\tan\lambda_1 L - \lambda_1 L)\}(y/b) + \{\alpha_1(\tan\lambda_1 L - \lambda_1 L) + \alpha_2(\tan\lambda_2 L - \lambda_2 L)\}] + d[1 - (x/L)] \quad (36)$$

Buckling of HST Solar Array

Numerical calculations presented hereafter use data[6,7] for the HST solar arrays as shown in Table 1. The BiSTEM material is stainless steel.

Without Blanket Offset

Table 2 shows P_{cr} values of the HST solar array obtained by solving Eq. (30). When the average compressive axial force P agrees with these critical values, buckling of the whole solar array occurs. The minimum value of the buckling forces is predicted to be about 15 N, and this value is only slightly larger than the design value of the average axial force of a BiSTEM of 14.75 N as determined by the membrane tension F_x [see Eq. (3d)].

The lower two buckling modes are shown in Fig. 4. It is clear that the first buckling mode shown in Fig. 4a is dominated by the torsional deformation of the solar array. The deformation is not symmetric, so that the outer BiSTEM deflects a little more than the inner BiSTEM; the ratio of their tip deflections $w_2(L)/w_1(L)$ is 1.03. The second buckling mode (Fig. 4b) is predominantly bending including a small torsional deformation component. In this case the deflection of the outer BiSTEM is less than the inner BiSTEM's deflection: $w_2(L)/w_1(L) = 0.95$. Coupling between bending and torsional deformations is more marked in the higher buckling modes not shown here.

Variations of the buckling forces were computed for variations of the difference $\Delta b = (b_2 - b_1)/2$, assuming the width of the solar blanket $b_1 + b_2$ to be constant. These results (not shown) indicate that the torsional buckling force rises and the bending buckling force falls with increasing Δb.

Table 1 Solar array properties of the HST

Half spreader bar width	$b = 1.4283$ m
Solar blanket width	$b_1 + b_2$
	$b_1 = 1.1383$ m
	$b_2 = 1.2493$ m
Solar array length	$L = 5.91$ m
Offset of solar blanket	$d = 0.0$ or 0.0376 m
Wall thickness	$h = 2.35 \times 10^{-4}$ m
Radius	$R = 1.092 \times 10^{-2}$ m
Bending stiffness	$EI = 1.711 \times 10^{2}$ N·m^2
Warping rigidity	$E\Gamma = 4.991 \times 10^{-1}$ N·m^4
Torsional rigidity	$GJ = 6.503 \times 10^{-3}$ N·m^2
Cross-sectional area	$A = 1.613 \times 10^{-5}$ m^2
Polar moment of inertia	$I_E = 1.948 \times 10^{-9}$ m^4
Coefficient of thermal expansion	$\alpha = 1.629 \times 10^{-5}$ 1/K
Thermal absorptivity	$\alpha_s = 0.5$
Thermal emissivity	$\varepsilon_s = 0.13$
Solar heat flux	$s_0 = 1.350 \times 10^{3}$ W/m^2
Specific heat	$c = 5.020 \times 10^{2}$ J/(kg·K)
Thermal conductivity	$k = 1.661 \times 10^{1}$ W/(m·K)
Density	$\rho = 7.010 \times 10^{3}$ kg/m^3
Stefan–Boltzmann constant	$\sigma = 5.670 \times 10^{-8}$ W/(m^2·K^4)

Table 2 Buckling forces of HST solar array

Mode	Buckling force P_{cr}, N
First	14.9916
Second	48.3406
Third	111.852
Fourth	193.363
Fifth	305.421
Sixth	435.070

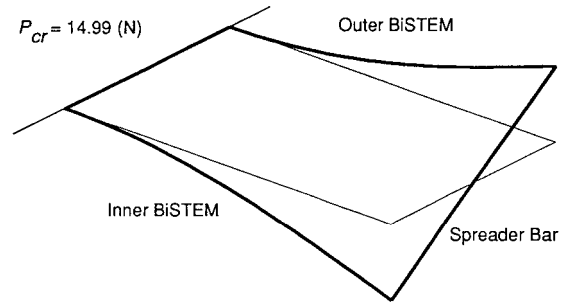

a) First mode

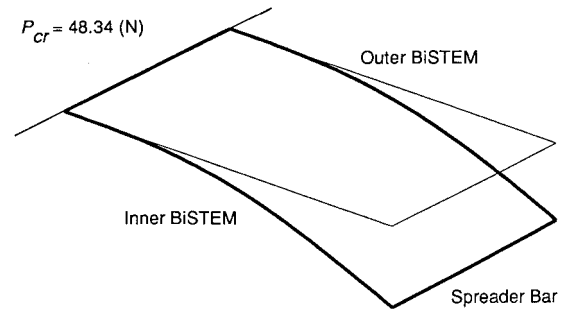

b) Second mode

Fig. 4 Lower two buckling modes of HST solar array.

With Blanket Offset

Tip deflections of the BiSTEMs computed including the out-of-plane offset d of the fixed end of the solar blanket are shown in Fig. 5. This result shows the variation of the tip deflections as the average compressive axial force P of the BiSTEMs increases. If P is small, bending deformation of the whole solar array occurs. As P increases to P_{cr}, torsional deformation becomes dominant. As P approaches P_{cr} from below, the deflection due to torsion becomes much larger

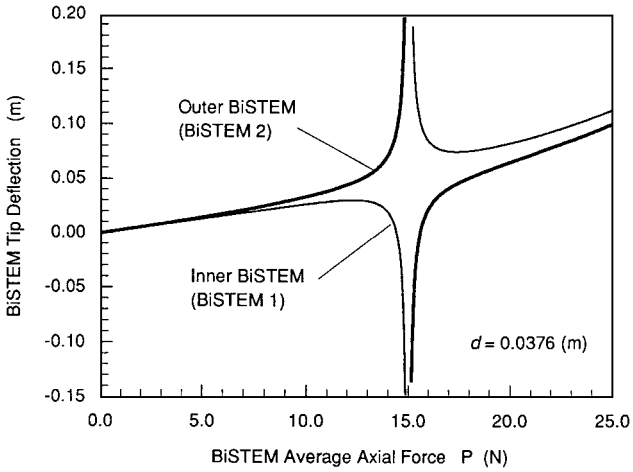

Fig. 5 BiSTEM tip deflections due to out-of-plane offset of solar blanket.

than the bending deflection. The tip deflections occur in opposite directions, and the tip deflection of the inner BiSTEM becomes negative. Because we can calculate the deflections due to the offset d except when $P = P_{cr}$, the results are shown also for P larger than P_{cr}. It is interesting that the theory predicts the direction of the torsional deformation to be reversed when the average compressive axial force is larger than P_{cr}.

Thermal Analysis

In the uncoupled thermal–structural analyses shown hereafter, the temperature distribution is assumed to be independent of structural deformations. The thermal analysis is presented in Refs. 4, 8, and 9. The solar array is subjected to an incident solar heat flux s_0 from the positive z direction that varies as a step function with time. The incident flux s_0 is assumed to be constant for time $t > 0$. Earth emitted and reflected radiation heatings are neglected. The thin-walled circular section boom, which is a simple model of the BiSTEM, is idealized by the following assumptions: 1) Radiation heating is uniform along the boom length, and heat conduction along the boom length is negligible; 2) the boom wall thickness is so small that the temperature gradient across it can be neglected; 3) radiation heat transfer inside the boom is negligible; and 4) thermal properties are assumed to be constant. With these assumptions, the temperature distribution is a function of time t and the angular coordinate χ of the boom cross section. The temperature distribution is represented as the sum of an average temperature $\bar{T}_i(t)$ and a perturbation temperature $T_{mi}(t)\cos\chi$, that is,

$$T_i(\chi, t) = \bar{T}_i(t) + T_{mi}(t)\cos\chi \tag{37}$$

The perturbation temperature that varies around the tube circumference induces a thermal bending moment that causes the BiSTEM boom to bend. References 4, 8, and 9 show that

$$T_{mi}(t) = T^*(1 - e^{-t/\upsilon}) \tag{38}$$

where

$$T^* = \tfrac{1}{2}(\alpha_s s_0/\rho ch)\upsilon$$
$$1/\upsilon = (k/\rho c R^2) + (4\varepsilon_s\sigma/\rho ch)[(1/\pi)(\alpha_s s_0/\varepsilon_s\sigma)]^{\frac{3}{4}} \tag{39}$$

The temperature T^* is the steady-state value of the perturbation temperature, and the parameter υ is a characteristic thermal response time.

Quasistatic Thermal–Structural Response

We now consider the thermal–structural response of the solar array when both BiSTEM booms are subjected to the same uniform radiation heating. Here, the quasistatic thermal response neglecting structural inertial forces is determined. In this case, the equations and boundary conditions for the BiSTEM bending and torsion and solar blanket deflection can be expressed in a manner similar to that of the buckling analysis. First, the partial differential equations and the boundary conditions for BiSTEM bending are

$$EI\frac{\partial^4 w_i}{\partial x^4} + P_i\frac{\partial^2 w_i}{\partial x^2} + \frac{\partial^2 M_T}{\partial x^2} = 0, \qquad i = 1, 2 \tag{40}$$

$$w_i(0, t) = 0, \qquad \frac{\partial w_i}{\partial x}(0, t) = 0, \qquad M_i(L, t) = 0 \tag{41}$$

where M_i is defined by

$$M_i = -EI\frac{\partial^2 w_i}{\partial x^2} - M_T \tag{42a}$$

and M_T is defined as an integration over a cross section by

$$M_T = \int_A E\alpha T z\, \mathrm{d}A \tag{42b}$$

After substituting the perturbation temperature distribution equation (37), the thermal bending moment of a thin-walled circular section boom is given as

$$M_T(t) = \frac{EI\alpha T_m(t)}{R} \tag{43}$$

where for a thin-walled circular section $I = \pi R^3 h$. Because we assume that the two BiSTEM booms are subjected to the same radiation heating, the temperature distributions of the BiSTEMs are identical. Then we can omit the subscript i for the temperature distribution T and the perturbation temperature T_m.

The partial differential equation and the boundary conditions for the BiSTEM torsional deformation are the same as given in Eqs. (9) and (10), except that now θ_{xi} depends on x and t. When P_i is small, it is satisfactory to assume that the parameter β_i given by Eq. (12) satisfies $\beta_i^2 > 0$. The following formulations take $\beta_i^2 > 0$ unless otherwise specified. It is easy to obtain the solutions for $\beta_i^2 < 0$ by repeating the same procedure.

The equation and the boundary conditions for the solar blanket deflection including the effects of the offset d are presented as

$$F_x\frac{\partial^2 w_m}{\partial x^2} = 0 \tag{44}$$

$$w_m(0, y, t) = d, \qquad w_m(L, y, t) = w_{s0} + y\theta_{s0} \tag{45}$$

Each of these equations is solved subject to the corresponding boundary conditions considering the geometrical restraint conditions for the torsional angle of the BiSTEM tip [Eq. (13)] and the relations between the deflection and rotation of the rigid spreader bar and the BiSTEM tip deflections [Eq. (18)]. Next, we express both the force and the moment equilibrium equations of the spreader bar in the same manner as the formulation of the buckling analysis using these results. Then the following simultaneous equations for the parameter α_i, which determine the magnitude of the BiSTEM deflections, are obtained:

$$\begin{bmatrix} C_{11}(P) & C_{12}(P) \\ C_{21}(P) & C_{22}(P) \end{bmatrix}\begin{Bmatrix} \alpha_1 \\ \alpha_2 \end{Bmatrix} = \begin{Bmatrix} g_1 \\ g_2 \end{Bmatrix} \tag{46}$$

where each term of the coefficient matrix is defined by Eqs. (24) and (28). The terms on the right-hand side of the equation are defined as

$$g_1 = \frac{M_T}{L}\left(\frac{1 - \cos\lambda_1 L}{\cos\lambda_1 L} + \frac{1 - \cos\lambda_2 L}{\cos\lambda_2 L}\right) + 2P\frac{d}{L} \tag{47a}$$

$$g_2 = \frac{M_T b}{L}\left\{\frac{1}{P_{f1}}\frac{1-\cos\lambda_1 L}{\cos\lambda_1 L}\left(\frac{b_2^2 - b_1 b_2 + b_1^2}{3b^2} - \frac{b_2 - b_1}{2b}\right)\right.$$

$$\left. - \frac{1}{P_{f2}}\frac{1-\cos\lambda_2 L}{\cos\lambda_2 L}\left(\frac{b_2^2 - b_1 b_2 + b_1^2}{3b^2} + \frac{b_2 - b_1}{2b}\right)\right\}$$

$$- \frac{M_T}{2Pb}\left(\frac{1}{P_{f2}}\frac{1-\cos\lambda_2 L}{\cos\lambda_2 L} - \frac{1}{P_{f1}}\frac{1-\cos\lambda_1 L}{\cos\lambda_1 L}\right)$$

$$\times \sum_{i=1}^{2}\left(GJ - P_{fi}\frac{PI_E}{A}\right)\frac{\beta_i \sinh\beta_i L}{\beta L \sinh\beta L + 2(1-\cosh\beta L)}$$

$$- 2Pb\frac{d}{L}\frac{b_2 - b_1}{2b} \tag{47b}$$

Unless the average P is equal to P_{cr}, the value of α_i is obtained by solving Eq. (46):

$$\begin{Bmatrix}\alpha_1\\ \alpha_2\end{Bmatrix} = \frac{1}{C_{11}C_{22} - C_{12}C_{21}}\begin{Bmatrix}C_{22}g_1 - C_{12}g_2\\ \dagger - C_{21}g_1 + C_{11}g_2\end{Bmatrix} \tag{48}$$

The deflections and the angles of twist of the BiSTEMs are

$$w_i(x,t) = \alpha_i\{\tan\lambda_i L(1-\cos\lambda_i x) - (\lambda_i x - \sin\lambda_i x)\}$$

$$- \frac{M_T}{P}\frac{1}{P_{fi}}\frac{1-\cos\lambda_i x}{\cos\lambda_i L} \tag{49}$$

$$\theta_{xi}(x) = \gamma_i\{\sinh\beta_i L(\sinh\beta_i x - \beta_i x)$$

$$-(1-\cosh\beta_i L)(1-\cosh\beta_i x)\} \tag{50a}$$

where

$$\gamma_i = -\frac{\theta_{s0}}{\beta_i L \sinh\beta_i L + 2(1-\cosh\beta_i L)} \tag{50b}$$

The numerator is the BiSTEM tip angle of twist. It is given by

$$\theta_{s0} = \theta_{xi}(L,t) = \frac{1}{2b}\{\alpha_2(\tan\lambda_2 L - \lambda_2 L) - \alpha_1(\tan\lambda_1 L - \lambda_1 L)\}$$

$$- \frac{M_T}{2Pb}\left(\frac{1}{P_{f2}}\frac{1-\cos\lambda_2 L}{\cos\lambda_2 L} - \frac{1}{P_{f1}}\frac{1-\cos\lambda_1 L}{\cos\lambda_1 L}\right) \tag{50c}$$

The solar blanket deflection is written as

$$w_m(x,y,t) = (x/L)(w_{s0} + y\theta_{s0}) + d[1-(x/L)] \tag{50d}$$

where the deflection of the center of mass of the spreader bar w_{s0} is given by

$$w_{s0} = \frac{1}{2}\{\alpha_1(\tan\lambda_1 L - \lambda_1 L) + \alpha_2(\tan\lambda_2 L - \lambda_2 L)\}$$

$$- \frac{M_T}{2P}\left(\frac{1}{P_{f1}}\frac{1-\cos\lambda_1 L}{\cos\lambda_1 L} + \frac{1}{P_{f2}}\frac{1-\cos\lambda_2 L}{\cos\lambda_2 L}\right) \tag{50e}$$

As shown in Eq. (42), we can calculate the bending moment distribution of the BiSTEMs using the deflection distributions. Thus, substituting Eq. (49) into Eq. (42a) permits us to write M_i as

$$M_i = P_{fi}P\alpha_i(\sin\lambda_i x - \tan\lambda_i L\cos\lambda_i x)$$

$$- M_T\left(1 - \frac{\cos\lambda_i x}{\cos\lambda_i L}\right) \tag{51}$$

To obtain the location where the maximum bending moment occurs, let the partial derivative of the preceding equation with respect to x be equal to zero and solve it for x. The location x_m of the maximum bending moment of the BiSTEM is given by

$$\frac{x_m}{L} = \frac{1}{\lambda_i L}\tan^{-1}\frac{P_{fi}P\alpha_i\cos\lambda_i L}{M_T - P_{fi}P\alpha_i\sin\lambda_i L} \tag{52}$$

If the dimensionless value x_m/L calculated by the equation has a value other than between 0 and 1, the maximum bending moment occurs at the fixed end of the BiSTEM.

Quasistatic Response of HST Solar Array

It is expected that structural responses vary significantly with P. First, Fig. 6a shows time histories of the BiSTEM tip deflections when the average compressive axial force P takes the design value 14.75 N. The horizontal axis uses a nondimensional time with the characteristic thermal response time $\upsilon = 23.8$ s. Because the temperature difference between the heated and the unheated sides increases with time, as shown in Eq. (38), the deflections also increase with time. Figure 6a shows that deflections of the outer and the inner BiSTEMs are different in spite of the uniform heating, due to the torsional deformation. Figure 6b shows time histories of the maximum bending moments of the BiSTEMs. The location where the maximum bending moment occurs is calculated by Eq. (52) and is independent of time. The larger bending moment occurs on the outer BiSTEM, and the maximum bending moment location is about 34% of the length from the fixed end. Figure 7 shows distributions of the steady-state deflections and bending moments of the BiSTEMs along the length. The results show that the torsion causes a large deflection and bending moment of the outer BiSTEM.

Next, we examine the variation of the quasistatic structural response with the average P. Because time histories are considered to be essentially similar to the results shown in Fig. 6, we consider the steady-state deflections and bending moments of the BiSTEMs. Figure 8 shows variations of tip deflections and tip rotation angle, which is equal to the rotation angle of the spreader bar, of the BiSTEM with P. Because the deformations are almost pure bending when P is small, the figures are shown for $P > 12$ N. It is clearly

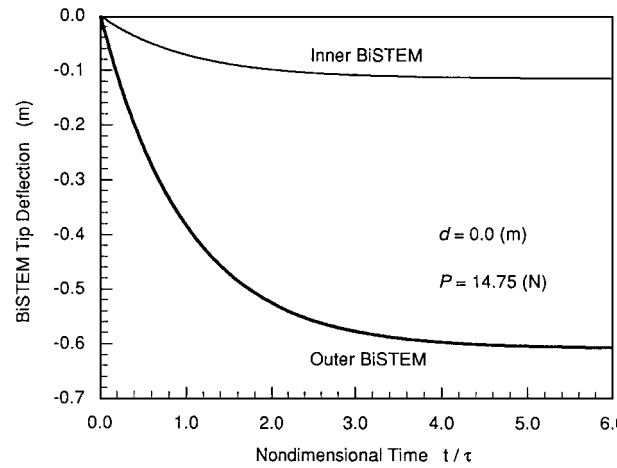

a) Tip deflections

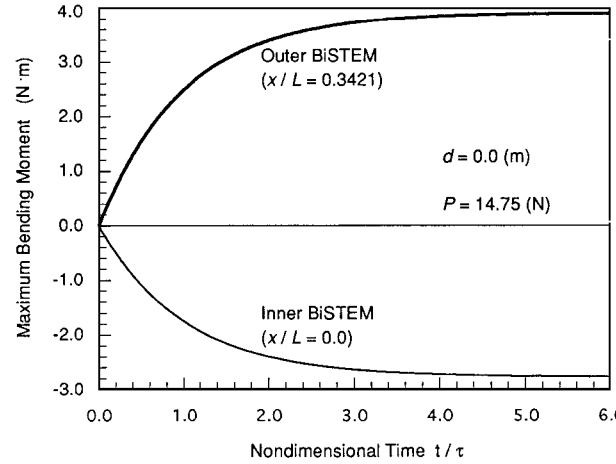

b) Maximum bending moments

Fig. 6 Time histories of quasistatic responses of HST solar array subject to uniform radiation heating.

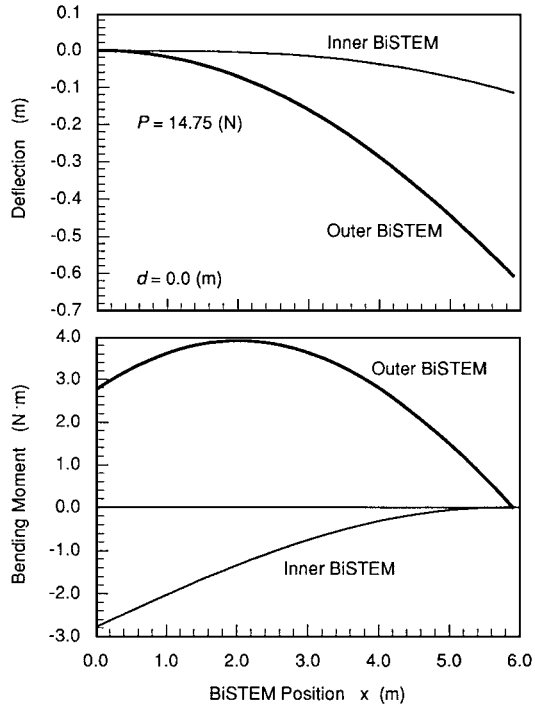

Fig. 7 Steady-state distributions of deflections and bending moments of BiSTEM.

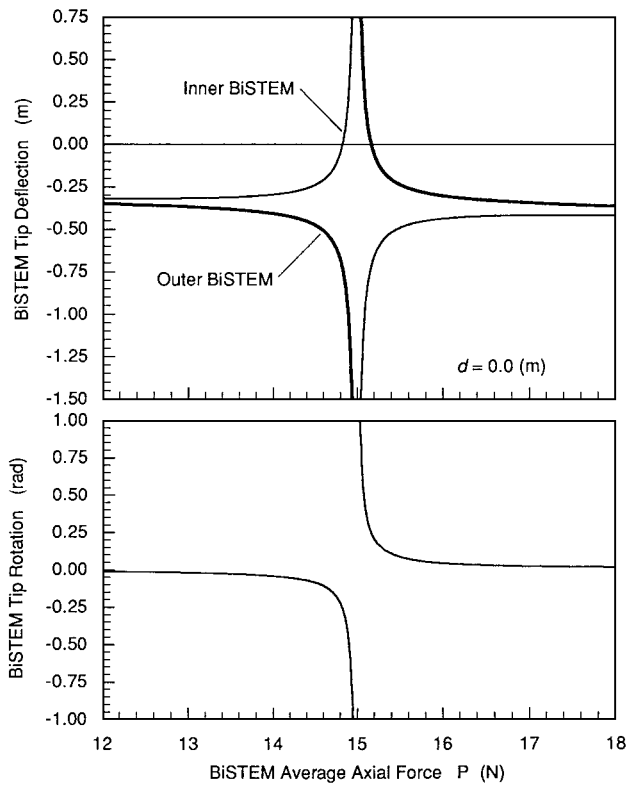

Fig. 8 Variations of tip deflections and rotation with average axial force of BiSTEM.

shown that, as P approaches P_{cr}, torsional deformation becomes dominant, similar to the deflection due to the offset d (see Fig. 5).

Variations of the steady-state deflections and bending moments of the BiSTEMs with the average axial force are shown in Fig. 9. Figure 9a shows the deflections of the BiSTEM. When P is smaller than about 14.0 N, bending deformation is dominant. But if P exceeds about 14.5 N, torsional deformation becomes dominant, and the magnitudes of the deformations are strongly dependent on P. Figure 9b shows bending moment distributions of the BiSTEM along their axis for the average axial force close to the critical buckling force. Large bending moments occur, especially on the outer

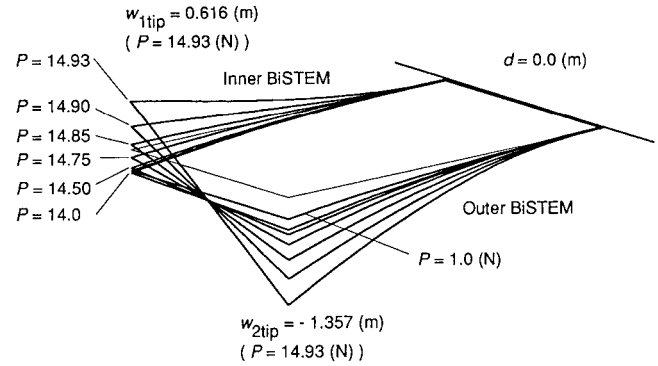

a) BiSTEM deflection

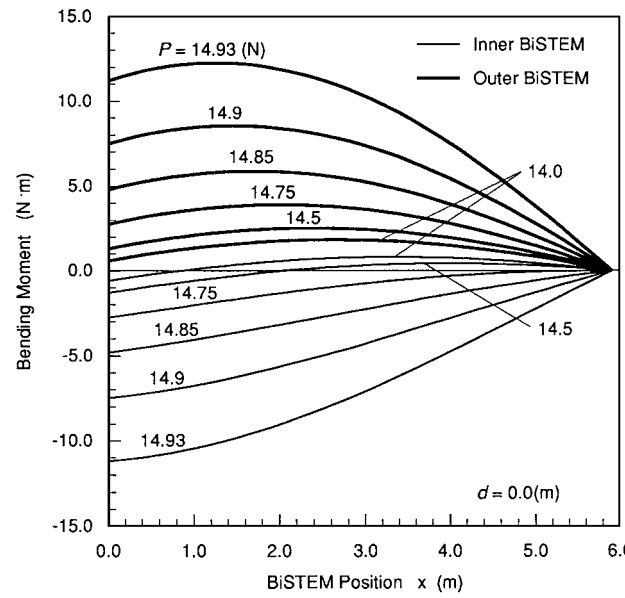

b) Bending moment

Fig. 9 Changes of steady-state responses of HST solar array with average axial force.

BiSTEM at 20–40% of the length from the fixed end. This maximum bending location agrees with the position where photographs show the failure occurred. According to Ref. 6, maximum bending moments for the acceptance and ultimate static load tests applied to the BiSTEM are 3.93 and 7.69 N · m, respectively. Reference 6 showed that a BiSTEM could withstand a bending moment of 12.15 N · m without failure. The present analysis shows that, if the solar array was subjected to radiation heating with the compressive axial force P near the critical buckling force P_{cr} for torsion, then failure of the outer BiSTEM of the solar array is likely to occur in a manner consistent with results in the astronauts' photographs.

Conclusions

Theoretical analyses of the buckling characteristics and the quasistatic thermal–structural responses of an asymmetric flexible rolled-up solar array were presented. The analyses were based on a generalized flexible rolled-up solar array model assuming asymmetric loading conditions because of geometric asymmetry. Numerical calculations were conducted using the data for the solar arrays of the HST.

The buckling analysis established the possible critical buckling forces and buckling modes and showed that, for the HST solar array, buckling will occur in torsion. The lowest buckling force was slightly larger than the typical design value of the solar array. Though all buckling modes were influenced by the bending–torsional coupling, the first mode was dominated by torsional deformation, the second was bending, and the higher modes were affected considerably by the coupling. Calculated results also suggested that the torsional buckling force rose and the bending buckling force fell because of the bending–torsion coupling effects.

The effects of the out-of-plane offset of the fixed supported end of the solar blanket on the bending-torsional coupling deformations of the solar array were investigated. The results showed that bending deformations of the whole solar array occur if the compressive axial force of the BiSTEM is small, but torsional deformations became dominant as the axial force increased to the critical buckling force.

Quasistatic structural responses of the solar array subjected to sudden radiation heating such as typical night–day transition in orbit were also presented. Both time histories and steady-state distributions of deflections and bending moments of the HST solar array were calculated. The results showed that the structural response depends significantly on the compressive axial force. When the axial force was close to the buckling force, large bending moments occurred at the midpoint of the outer BiSTEM. The values of the calculated maximum bending moments were as large as the design ultimate value when the axial force was close to the critical buckling force. This result suggests that thermally induced quasistatic torsional deformation may have caused the failure of the solar array BiSTEM.

References

[1]Fortescue, P., and Stark, J. (ed.), *Spacecraft Systems Engineering*, 2nd ed., Wiley, New York, 1995, cover photograph.

[2]Petersen, C. C., and Brandt, J. C., *Hubble Vision: Astronomy with the Hubble Space Telescope*, Cambridge Univ. Press, New York, 1995, p. 37.

[3]Chaisson, E. J., *The Hubble Wars*, Harper Collins, New York, 1994, pp. 92–97.

[4]Thornton, E. A., and Kim, Y. A., "Thermally Induced Bending Vibrations of a Flexible Rolled-Up Solar Array," *Journal of Spacecraft and Rockets*, Vol. 30, No. 4, 1993, pp. 438–448.

[5]Chung, P. W., and Thornton, E. A., "Torsional Buckling and Vibrations of a Flexible Rolled-Up Solar Array," AIAA Paper 95-1355, April 1995.

[6]Reynolds, J., "The Analysis of the Deployed Space Telescope Solar Array," European Space Agency, ESA Doc. TN-SA-B142, British Aerospace, Bristol, England, UK, Jan. 1983.

[7]"STEM Design Characteristics and Parameters," Astro Aerospace Corp., TR AAC-B-006, Carpinteria, CA, Sept. 1985.

[8]Rimrott, F. P. J., and Abdel-Sayed, R., "Flexural Thermal Flutter Under Laboratory Conditions," *Transactions of the Canadian Society for Mechanical Engineering*, Vol. 4, No. 4, 1977, pp. 189–196.

[9]Murozono, M., and Sumi, S., "Thermally Induced Bending Vibration of Thin-Walled Boom with Closed Section by Radiant Heating," *Memoirs of the Faculty of Engineering, Kyushu University*, Vol. 49, No. 4, 1989, pp. 273–290.

H. L. McManus
Associate Editor